J Porous Mater (2017) 24:631–638
DOI 10.1007/s10934-016-0299-4

Synthesis and characterization of SBA-15 modified with alkali metals

L. A. Cano[1] · M. V. Cagnoli[1] · J. F. Bengoa[1] · J. L. Garcia-Fierro[2] · S. G. Marchetti[1]

Published online: 7 October 2016

Abstract A synthesis protocol that has not been previously reported in the literature that allows doping a solid of SBA-15 with alkali metals, preserving the structural features of the mesoporous solid has been developed. X-ray diffraction at low angles, Nitrogen adsorption, Electron transmission microscopy, X-ray photoelectron spectra, atomic absorption spectroscopy and Thermal Programmed Desorption of carbon dioxide were used to characterize the solids obtained. The introduction of alkali metals within the channels of the solid generates basic sites of weak and intermediate strength, which do not exist in undoped SBA-15. Without significant changes in the structural and textural properties of the support, only the densification of the channel walls is evidenced. According to the alkali metal used, the order established by the total number of sites obtained is: Li-SBA-15 $\gg$ K-SBA-15 $\approx$ Cs-SBA-15, while the order by force of both types of sites (weak and intermediate) is: Li-SBA-15 $>$ Cs-SBA-15 $>$ K-SBA-15.

Keywords Mesoporous materials · Alkaline cations · Basicity · Surface properties

✉ L. A. Cano
lcano@quimica.unlp.edu.ar

[1] CINDECA, CONICET, Fac. De Cs. Exactas, UNLP, 47 Y 115, La Plata, Argentina

[2] Instituto de Catálisis y Petroquímica, CSIC, Cantoblanco, 28049 Madrid, Spain

1 Introduction

The mesoporous materials with regular geometries have recently received much attention because of their potential in practical applications, such as catalysis, adsorption, separation, detection, medical use, ecology and nanotechnology [1–6]. The first reported synthesis of ordered mesoporous material called SBA-15 occurred in 1998, composed for silica walls with large and uniform mesoporous arranged in an array of two-dimensional (2-D) that can easily be obtained using a triblock polymer of polyethylene and polypropylene oxides as directing agent in a highly acid medium [7, 8]. An interesting property of this material is that its mesoporous are connected through complementary pores (microporous and small mesoporous) in the silica walls of the main pores. With very large pores and narrow pore-size distribution, whose diameters can be varied between 5 and 30 nm, wall thickness between 3 and 6 nm, and specific surface area between 700 and 1000 m^2/g, and a high hydrothermal stability, SBA-15 has potential promising applications in many fields, as it mentioned above [9–12]. Furthermore, the synthesis of SBA-15 and similarly structured materials can be obtained using a low cost silica source such as sodium silicate [13, 14], which makes this a commercially viable synthesis.

In the field of the solid catalyst SBA-15 is widely used as support for heterogeneous catalysts because their large surface area promotes a high and homogeneous dispersion of the active species. When this support is used in oxidation reactions of alkanes and alkenes [15–17] and in the Fischer–Tropsch synthesis [18–20] it is necessary to generate basic sites that promote the activity, stability and selectivity of the catalysts.

For example, in CO hydrogenation, alkali metals have been widely studied as promoters to increase the activity

and selectivity, besides, when in contact with a transition metal may alter the binding energies and the adsorption capacity of the reactive molecules [21]. According with Lee and Ponec [22] CO dissociation velocity and the dispersion of the active metal on the support are incremented by adding the alkaline promoters. Alkali metals of the first group of the periodic table, like: Li, Na, K, Rb and Cs are the most used promoters [23].

The alkali metals must be located within the pores of the support and additionally, it is crucial avoid the introduction of dopants that can alter the structural properties of the support. In the literature there are practically no results that solve these problems. Thus, recently a few published articles appeared, trying to solve some of these problems by using two approaches: (a) impregnation of SBA-15 with aqueous alkali metal salts (acetates, carbonates, nitrates) and subsequent calcination [15, 24] and (b) incorporation of the same salts in the synthesis gel SBA-15 and subsequent calcination [25, 26] .

In this paper we propose the synthesize SBA-15 support doped with different alkali metals Li, K and Cs, to increase the basicity of the support.

The challenge of this paper is to withhold the metals within the channels, without substantial changes in the mesoporous solids.

2 Experimental

2.1 Samples preparation

The SBA-15 support was synthesized according to the methodology proposed by Zhao et al. [7, 8] using Pluronic triblock copolymer P123 (EO20-PO70-EO20) as organic structure-directing agent and tetraethyl orthosilicate (TEOS) as silica source. Thus, 12 g of Pluronic P123 were dissolved in 360 ml of water and 60 ml of HCl solution (37 % w/w) with stirring at 313 K for 3 h. Then, 27 ml of TEOS were added, and the solution was kept stirring at 313 K for 24 h. The mixture was aged at 363 K overnight, without stirring. The solid was recovered by filtration, washed, and dried in air at room temperature (RT). Calcination in air was carried out from RT to 773 K at 1 K/min and kept at 773 K for 6 h.

The SBA-15 modified with alkaline metals was prepared using the same methodology as described above. The only difference was that $CsNO_3$ or KNO_3 or $LiNO_3$ were added with the P123 and the final solid was not recovered by filtration and washed. All water remaining in the synthesis gel was eliminated by evaporation at 333 K and vacuum. The amount of alkali metal added in each case was calculated in order to maintain an atomic ratio M/Si = 0.0125. Thus, every 12 g of P123 we added 0.102 g of $LiNO_3$ or 0.15 g of KNO_3 or 0.295 g of $CsNO_3$. The solids were denoted as Li-SBA-15, K-SBA-15 and Cs-SBA-15.

2.2 Samples characterization

The samples were characterized by X-ray diffraction (XRD) at low angles, N_2 adsorption (BET), Electron transmission microscopy (TEM), X-ray photoelectron spectra (XPS), atomic absorption spectroscopy (AAS) and Thermal Programmed Desorption (TPD) of CO_2.

The X-ray diffraction patterns at low angles were recorded in Shimadzu equipment, XD3A model, using Cu Kα radiation generated at 40 kV and 40 mA in the range 2 h = 0.5–90° with steps of 0.02° and counting time of 2 s/step.

The textural properties, specific surface area (Sg), specific pore volume (Vp) and pore diameter (Dp), were measured in Micromeritics equipment ASAP 2020 V1.02 E.

Samples for TEM analysis were prepared by drying a dispersion of the solids on amorphous carbon coated copper grids. TEM micrographies were obtained on a JEOL Model JEM-1200 EX II Instrument microscope.

The XPS were performed in a VG ESCALAB 200R (Fisons). It offers a source of X-ray emission dual anode Mg–Kα (1253.6 eV) and Al-Kα (1486.6 eV), operating at 12 kV and 10 mA. It is equipped with a hemispherical analyzer and five channeltron detectors type. The working pressure in the analysis chamber was always less than 5×10^{-8} mbar. The recording of the spectra was performed in a window of energies 10–20 eV and sufficient spectra (30–500) were accumulated to get a good signal/noise ratio. The binding energies are referred to the Al 2p level (73.9 eV).

The alkaline metal content of the solids was determined by atomic absorption on an AA/AE Spectrophotometer 457 of Laboratory Instrumentation Inc. The samples were attacked in a mixture of HCl and HF up to complete dissolution and then were treated according to conventional methods for this technique.

The TPD-CO_2 analyses were carried out in a stainless steel fixed-bed reactor (2.54 cm o.d.). The sample was activated in an Ar stream (20 cm^3/min) at 973 K during 2 h. Then a CO_2/Ar (8:100) stream passed through the sample during 5 min and was flushed by pure Ar to eliminate the CO_2. After that, the solid was heated in an Ar flow with a heating rate of 10 K/min up to 973 K in order to desorb the CO_2. This gas flow was mixed with a H_2 flow (20 cm^3/min) and passed through a Ni/SiO_2 catalyst at 673 K to convert CO_2 into CH_4 which was quantified using a FID detector. In this way the amount of adsorbed CO_2 was determined.

3 Results and discussion

The porous structure of the hexagonal solid SBA-15 has a characteristic XRD pattern at low diffraction angles. According to the literature, there are three diffraction lines at $2\theta = 0.9$, 1.6 and 1.8° corresponding to (100), (110) and (200) planes, associated with the hexagonal symmetry of SBA-15 [7, 8]. The X-ray diffraction patterns at low angles of SBA-15 and the impregnated supports (Li-SBA-15, K-SBA-15 and Cs-SBA-15) are displayed in Fig. 1. The three lines described above can clearly be differentiated in all diffractograms. The intensity of the first line (100 plane) gives an indication of the high symmetry of the solid obtained and the presence of the two peaks at higher angles show a high frequency in the structure.

The positions of the diffraction peaks are coincident, with very slight differences, with those published in the literature, which shows that there are no major changes in the solid structure after incorporating the alkali metals.

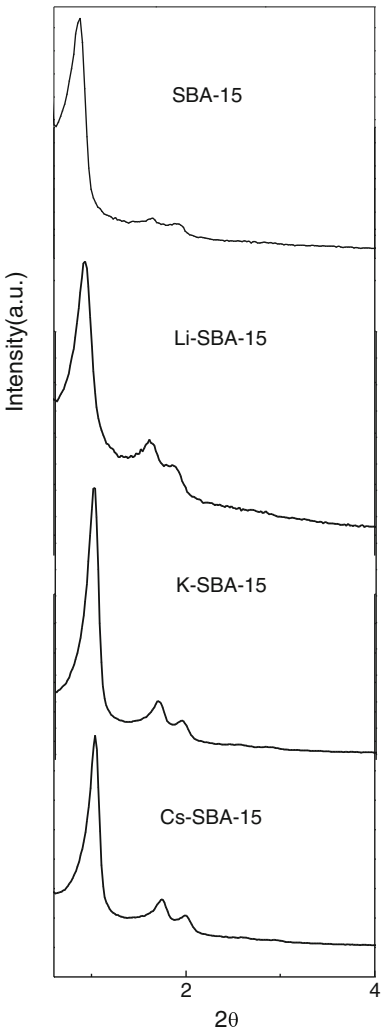

Fig. 1 XRD at low angles of the mesoporous solids

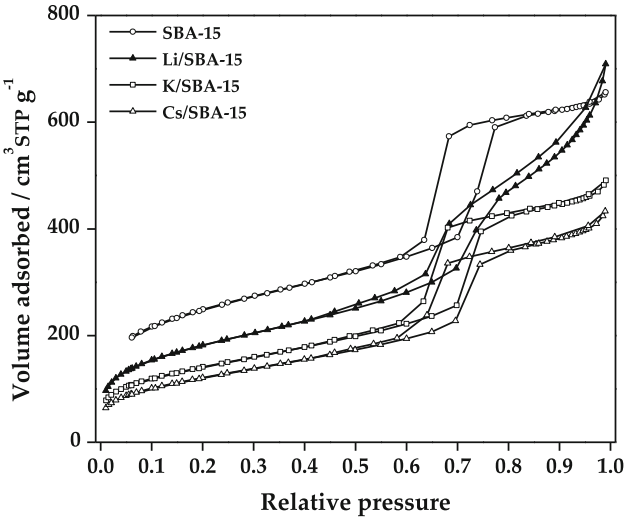

Fig. 2 N_2 isotherms of mesoporous solids

Table 1 Textural properties of the mesoporous solids

Sample	S_g (m^2/g)	V_p (cm^3/g)	r_p (nm)	t (nm)
SBA-15	893	1.09	4.1	6.8
Li-SBA-15	653	0.98	4	2.3
K-SBA-15	529	0.75	4.1	2.1
Cs-SBA-15	435	0.61	3.5	2.8

Only in the doped SBA-15, the position of the most intense peak shows a slight shift towards larger angles compared with the solid undoped. Taking into account that the peak position in the 100 plane is inversely related to the interplanar distance, it can be concluded that the introduction of alkali metals produce the contraction network. Other authors have reported similar results [26].

Figure 2 displays the different N_2 adsorption–desorption curves of the synthesized solids. In all cases Type IV isotherms were obtained, which are characteristic of mesoporous solids with a narrow pore diameter distribution. Furthermore all solids exhibit H1 hysteresis type, which is characteristic of mesoporous materials with uniform pore size and shape. The sharp increase of N_2 adsorption at near saturation and slight distortion in the increased values of the hysteresis "loop" (most noticeable in the case of Li-SBA-15) would presume a slight tendency of the type H1 hysteresis towards to the H3 type [27]. However, in the three doped solids no significant differences were observed with respect to the undoped solid, thus we can conclude that the addition of alkali metal brought no consequences on the pore shape and their narrow size distribution.

From BET isotherms, the values of specific surface area (Sg), pore volume (Vp), pore radius (r_p) and wall thickness (t) of the channels were calculated. In Table 1 the values of these properties can be seen.

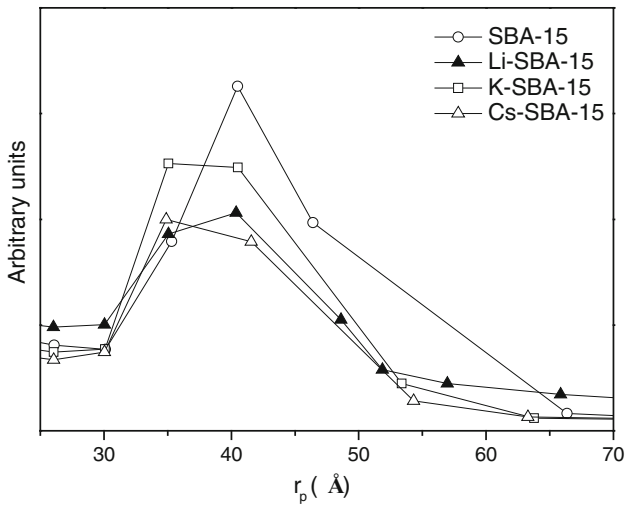

Fig. 3 Pore radius distribution of the solids

The solids obtained have specific surface areas between 400 and 700 m^2/g, pore volumes between 0.6 and 1 cm^3 and pore radius near 4 nm, typical values for this type of mesoporous solids. By comparing the values obtained for the undoped SBA-15 whit the doped solids, we can see that the differences are not very large and are within the range of expected values for these solids. The largest decrease in Sg and Vp values is observed for Cs-SBA-15, perhaps due to the higher alkali metal content in Cs-SBA-15 and the larger size of the basic cation. Table 1 displays that the pore radius values have not diminished in the same way as the specific volume and the specific surface area. This would indicate that when the alkali metals are added, a partial filling of the channels occurs. On the other hand, the wall thickness estimated for the support is substantially less than the computed for the undoped SBA-15. This is due to the contraction of the lattice parameter accompanied by a negligible change in the pore radius. It is possible to speculate that the alkali metal incorporation contracts the channel walls. A similar result was reported by Zhang et al. [26].

Using the model developed by Barrett, Joyner and Halenda, BJH method, the pore size distribution for each solid was calculated from the adsorption isotherms data. The results are shown in Fig. 3. Mesoporous solids with very narrow pore size distributions were obtained in all cases. The distribution width in the doped supports is very similar to that obtained for the undoped solid thus it can be concluded that introducing an alkali metal into the SBA-15 structure, no changes occur in the pore size distribution.

In Fig. 4 are shown the transmission electron micrographs of SBA-15 solids with different alkaline cations incorporated. These photos were taken in perpendicular direction to the axes of the channels of the solids. They can clearly distinguish the same characteristic cylindrical and uniforms channels of SBA-15 for all solids obtain. In the

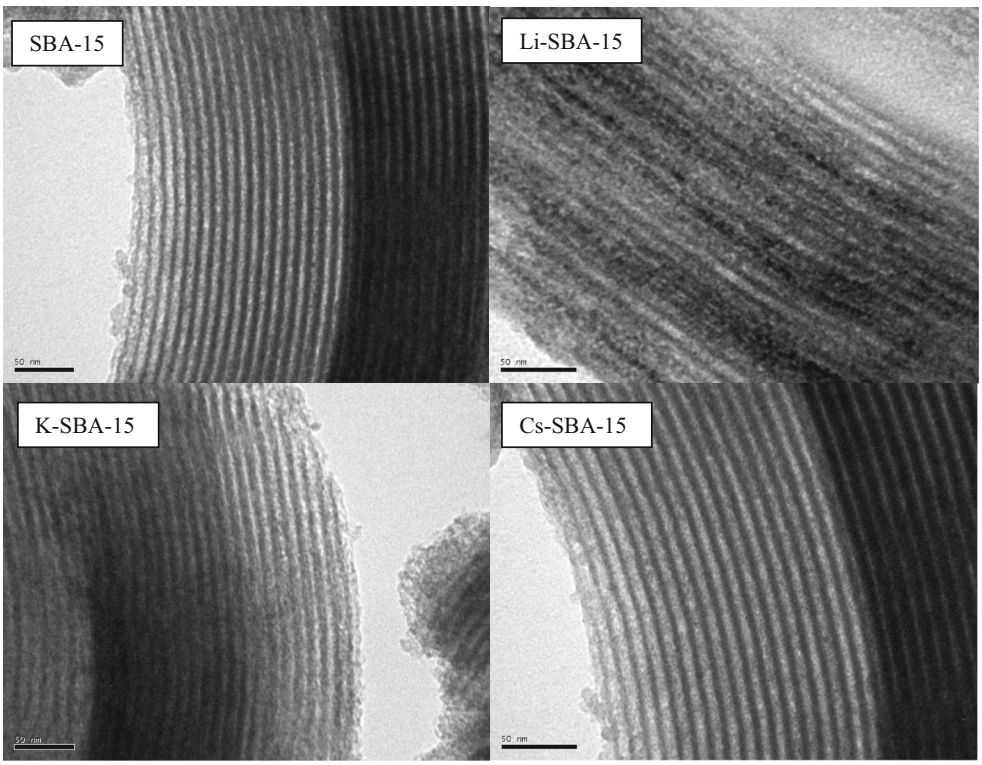

Fig. 4 Transmission electronic microscopy

Table 2 Metal content, binding energies and surface atomic ratios

Support	Alkali metal content (%w/w)	Binding energies of alkali metal (ev)	Surface atomic ratio (M/Si)
Li-SBA-15	0.11	Li 1 s = 55.1	0.315
K-SBA-15	0.4	K $2p_{3/2}$ = 293.4	0.009
Cs-SBA-15	2.17	Cs $3d_{5/2}$ = 725.1	0.004

photos the lightest parts are mentioned channels, while the darker parts are solid walls. A great uniformity in the sizes of the channels and a marked linearity thereof shown. Similar photos have been reported previously for these solids [28, 29]. These photographs are further input to the DRX confirmation at low angles and N_2 adsorption isotherms when verifying that the solid obtained SBA-15 with different alkaline cations incorporated have the typical characteristics previously reported in the literature.

In Table 2 the results of binding energies and surface atomic ratio obtained from XPS spectra (Fig. 5) in addition to the metal content incorporated into the support, measured by atomic absorption and emission can be seen.

Table 2 shows that it has been managed to introduce and maintain the alkali cations in the medium after all the

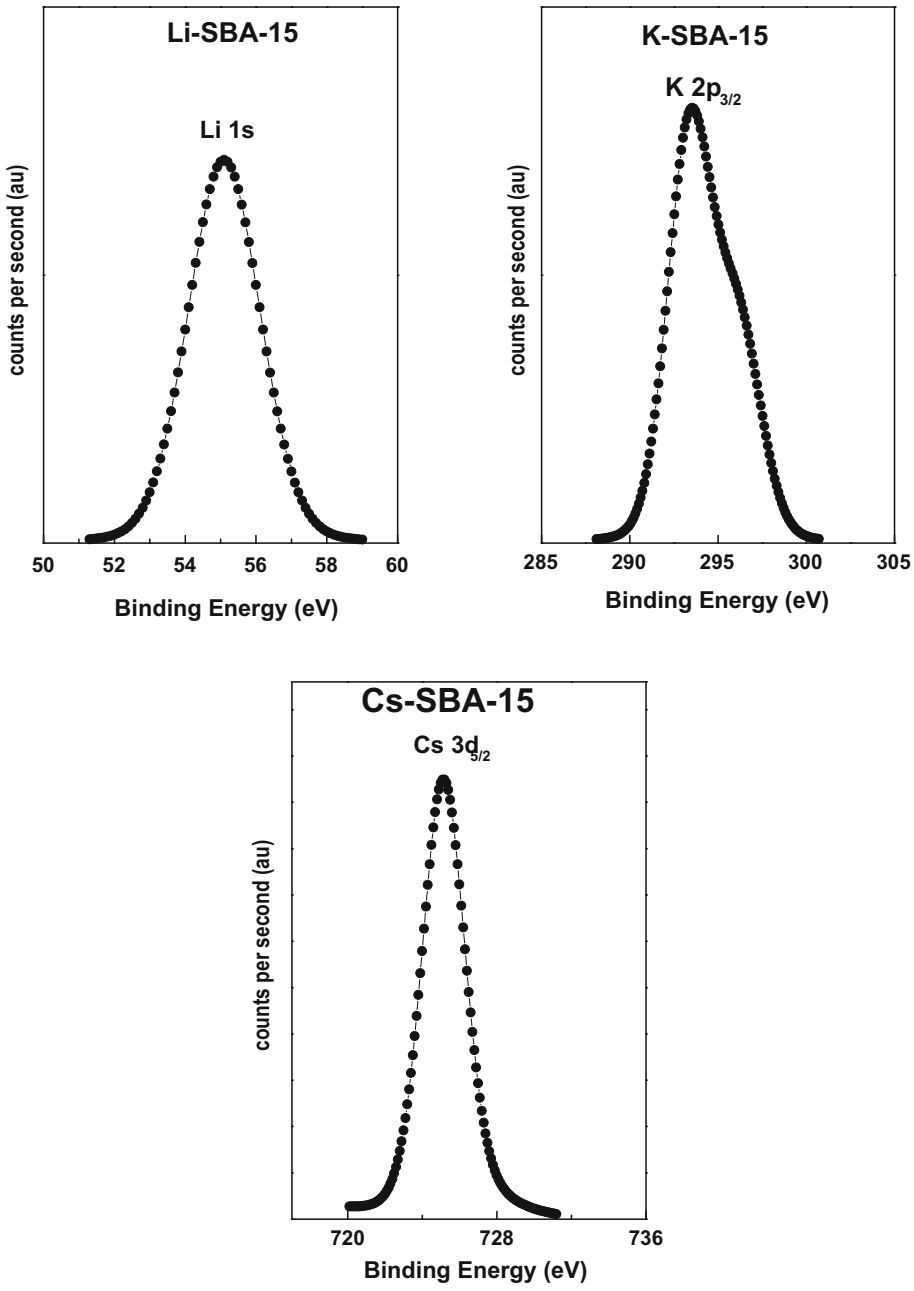

Fig. 5 X-ray photoelectron spectra of doped solids

preparation steps of the solids. Furthermore the contents obtained are very similar to the nominal values (0.11 % w/w of Li, 0.62 % w/w of K and 2.11 % w/w Cs).

In the case of the solid Li-SBA-15 the value of the binding energy of the 1 s Li close to 55 eV is typical of lithium oxide [30]. Analyzing the solid with potassium, it can be seen that its binding energy of the $2p_{3/2}$ level of the metal corresponds to KOH [31]. The binding energy value of Cs seems to correspond to species of $CsNO_3$ [32].

Therefore, it can be concluded that thermal treatments have been enough to decompose the nitrates of Li and K, although the oxide from the latter would have become KOH due to its hygroscopicity. In contrast, Cs salt was not decomposed.

It was not possible to confirm the assignment of these species using FT-IR spectroscopy due to the low concentration of the alkali metals and the presence of very intense bands of SBA-15 in characteristic adsorption regions.

Through the analysis of the surface atomic ratios, it can be seen that Li-SBA-15 has 35 times more of surface alkali metal atoms than the solid doped with K and 80 times more than the solid promoted with Cs. Then, a higher promoter basicity effect on Li-doped support would be expected.

Figure 6 displays the temperature programmed desorption curves for each doped support with the appropriate deconvolution using a nonlinear fit of minimum squares with two Gaussian peaks. It should be noted that the thermogram of the undoped solid SBA-15 has not presented CO_2 desorption peaks and its baseline was used to be deducted from each diagram of the doped supports. This denotes the absence of Lewis base sites in the undoped solid, as it was previously reported in the literature [15].

The thermograms of the three doped supports have two peaks corresponding to the CO_2 desorption at relatively low temperatures in the ranges of 340–380 and 380–460 K. These peaks correspond to CO_2 adsorbed on basic sites with different adsorption strength and will be called weak and intermediate sites. Whereas, as has been mentioned, the SBA-15 undoped not possess any of these sites, they may be attributed to the presence of alkali metals from Group 1 of the periodic table located in the support surface, in coincidence with some previous reports [15, 33, 34].

In Table 3 it can be observed that the support with the highest quantity of total superficial basic sites per gram of alkaline metal is Li-SBA-15, this quantity is approximately 20 times higher than in K-SBA-15 and 170 times higher than in Cs-SBA-15. These results cannot be explained by the mass content of each alkali metal, since K and Cs loadings are about 4 and 20 times higher than that of Li respectively. The CO_2 adsorption on alkaline and/or alkaline earth metals takes place under different species: bicarbonate, unidentate carbonates and bidentate carbonates [21–23]. The different adsorption ways reveal the

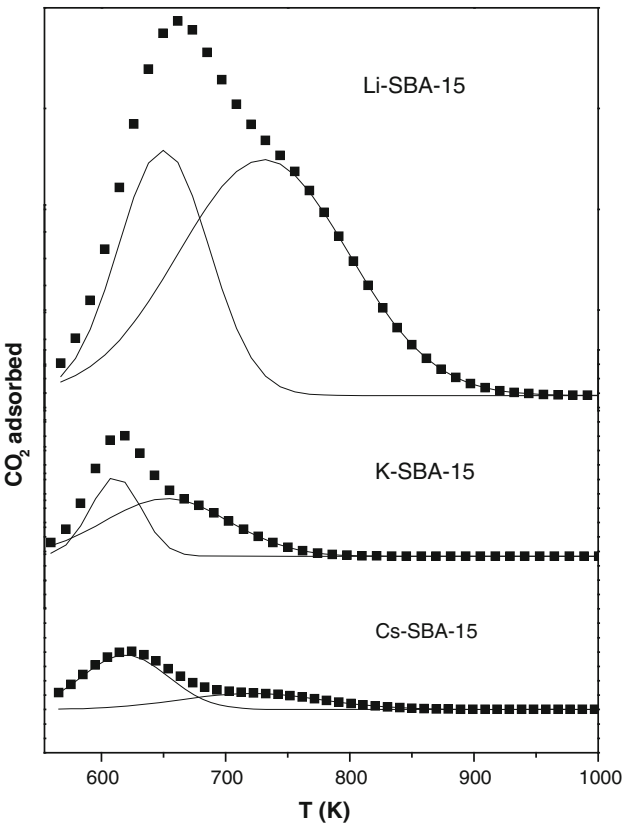

Fig. 6 TPD-CO_2 of the doped solids

different chemical nature of the oxygen atoms. Thus, for the unidentate carbonates formation, is necessary the presence of isolated O^{-2}, which are usually present on edges and vertices of small crystals. The bidentate carbonates are formed on pairs of Lewis acid/Brönsted basic (M^{+n}–O^{-2}) sites. Finally, bicarbonates species are related to superficial hydroxyls, which are the most labile of the three species. In general, the following strength order is proposed for superficial basic sites: isolated O^{-2} > M^{+n}–O^{-2} pairs > OH groups. Although in the present work these species had not been identified, it is known that one CO_2 molecule is adsorbed on a superficial alkaline metal atom. The following scheme represents this situation:

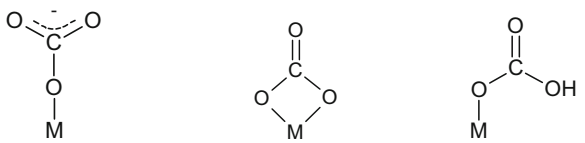

Monodentate carbonate Bidentate carbonate Bicarbonate

In this way, if the total amount of adsorbed CO_2 molecules per gram of solid is related to the total number

Table 3 Results obtained from the TPD - CO_2 essays of the supports

Support	$-q_0$ in M_2O	T (K)	W (K)	A_2/A_1	$\mu moles_{tot}/g_{MA}$	$D_M(\%)$
Li-SBA-15	0.80	377	73	1.78	4509	3.0
		458	136			
K-SBA-15	0.89	338	41	1.78	235	0.9
		379	101			
Cs-SBA-15	0.94	346	69	0.49	27	0.4
		448	114			

($-q_0$), Partial negative charge of oxygen in the alkali metal oxides; T, Temperature of maximum in desorption peak; W, width of desorption peak at half height; A_2/A_1, Area ratio of the second to the first peak of desorption; $\mu moles_{tot}/g_{MA}$: Total micromoles of CO_2 absorbed per gram of alkali metal; $D_M(\%)$, Alkali metal dispersion

of alkaline metal per gram of solid, an equivalent value to a dispersion could be obtained. This value will be independent of the amount of alkaline metal added to the sample. Table 3 shows that the Li-SBA-15 sample has a dispersion value 3 times higher than the K-SBA-15 sample and 7 times higher than the Cs-SBA-15 sample. These differences could be attributed to a higher agglomeration degree of the species when the size of the alkaline cations is higher and/or to an increase of the amount of alkaline ions located inside the walls of the SBA-15 (which are inaccessible to CO_2 molecules) when the size of the alkaline cations increases. The location inside the SBA-15 walls of an alkaline metal fraction is coherent with the change of the lattice parameter and with the higher density of the doped SBA-15. As it was previously discussed.

The maximum temperature and the peak width at half height can be used in order to obtain the desorption heat of CO_2. An increase in these values indicates a higher desorption heat and therefore a higher basic strength of the site where the CO_2 was adsorbed [26].

The basicity of a superficial oxide is generally related with the electro-donor properties of combined oxygen anions, thus, when the negative partial charge of this combined oxygen anions increases, the resultant oxide will be more basic. In this way, the oxygen negative partial charge ($-q_0$ in Table 3) would indicate the electron donor properties, in oxides with only component. These $-q_0$ values were calculated using the equalization of electronegativities principle [27], a decrease of $-q_0$ when atomic mass increases it can be observed. However, comparing the three supports obtained in this work, contrary to that expected it can be seen that the solid doped with Li displays the most basic strength for both weak and medium sites. Several authors [7, 30] have found that Li generates more basic sites and with higher strength, when is it used as solid dopant, than that expected.

The K-SBA-15 sample has adsorbed 8 times higher quantity of CO_2 per gram of metal loading than Cs-SBA-15; however, it has a metal content 5.4 times lower. Besides, both kind of sites generated by K are weaker than that produced by Cs, since their desorption peaks are sharp and appear at lower temperature that the ones corresponding to Cs-SBA-15. This result has also been reported by other author [31].

Another result is that the samples Li-SBA-15 and K-SBA-15 has a population of medium strength sites which is twice the population of weak strength sites (A_2/A_1 in Table 3), instead in Cs-SBA-15 this situation is inverted.

It can be observed that in the present work we generated superficial basic sites in a SBA-15 by adding alkaline metals, and the structural properties of the support were maintained.

The order established by the total number of sites obtained is: $Li \gg K \cong Cs$ and the order by basic strength of both types of sites: $Li > Cs > K$.

4 Conclusions

A new synthesis protocol that has not been previously reported in the literature, that allows to dope SBA-15 with alkali metals, preserving the structural features of the mesoporous solid has been reported.

The solids have specific surface area between 400 and 600 m^2/g, 8 nm of pore diameter and a wall thickness between 4 and 5 nm. The mesoporous solid has straight and uniform channels with hexagonally ordered.

The introduction of alkali metal within the channels of the solid did not produce significant changes in the structural and textural properties of the SBA-15, only the densification of the channel walls is evidenced.

Alkali metals incorporated into the support generated basic sites of weak and intermediate strength which do not exist in undoped SBA 15.

According to the alkali metal used, the order established by the total number of sites obtained is: $Li \gg K \cong Cs$, while the order by force of both types of sites (weak and intermediate) is: $Li > Cs > K$.

Acknowledgments The authors acknowledge the financial support of ANPCyT (PICT No. 22-38337 and 00549), which allowed the development of this work.

References

1. M.E. Davis, Nature **417**, 813 (2002)
2. A. Vinu, V. Murugesan, M. Hartmann, Chem. Mater. **15**, 1385 (2003)
3. A. Okabe, T. Fukushima, K. Ariga, M. Niki, T. Aida, J. Am. Chem. Soc. **126**, 9013 (2004)
4. K. Ariga, J. Nanosci. Nanotechnol. **4**, 23 (2004)
5. A. Taguchi, F. Schüth, Microporous Mesoporous Mater. **77**, 1 (2005)
6. A. Vinu, K.Z. Hossain, K. Ariga, J. Nanosci. Nanotechnol. **5**, 347 (2005)
7. D. Zhao, J. Feng, Q. Huo, N. Melosh, G.H. Fredrickson, B.F. Chmelka, G.D. Stucky, Science **279**, 548 (1998)
8. D. Zhao, Q. Huo, J. Feng, B.F. Chmelka, G.D. Stucky, J. Am. Chem. Soc. **120**, 6024 (1998)
9. S.-W. Kim, S.U. Son, S.I. Lee, T. Hyeon, Y.K. Chung, J. Am. Chem. Soc. **122**, 1550 (2000)
10. Y.S. Cho, J.C. Park, B. Lee, Y. Kim, J. Yi, Catal. Lett. **81**, 89 (2002)
11. Z. Zhang, S. Dai, D.A. Blom, J. Shen, Chem. Mater. **14**, 965 (2002)
12. X.Q. Wang, M. Wang, H.X. Jin, Z.H. Li, P.M. He, Appl. Surf. Sci. **243**, 151 (2005)
13. J.M. Kim, G.D. Stucky, Chem. Commun. **13**, 1159 (2000)
14. S.S. Kim, A. Karkamkar, T.J. Pinnavaia, M. Kruk, M. Jaroniec, J. Phys. Chem. B **105**, 7663 (2001)
15. S. Yang, W. Zhu, Q. Zhang, Y. Wang, J. Catal. **254**, 251 (2008)
16. A. Costine, T. O'Sullivan, B.K. Hodnett, Catal. Today **112**, 103 (2006)
17. H. Wang, Z. Zhao, Z. Zhang, A. Duan, C. Xu, J. Porous Mater. **15**, 221 (2008)
18. A. Martínez, C. López, F. Márquez, I. Díaz, J. Catal. **220**(2), 486 (2003)
19. D. Kim, B. Dunn, F. Huggins, G. Huffman, M. Kang, J. Yie, E. Eyring, Energy Fuels **20**, 2608 (2006)
20. L.A. Cano, M.V. Cagnoli, J.F. Bengoa, A.M. Alvarez, S.G. Marchetti, J. Catal. **278**(2), 310 (2011)
21. C. Wang, L. Xu, Q. Wang, J. Nat. Gas Chem. **12**, 10 (2003)
22. G. van der Lee, V. Ponec, Catal. Rev. Sci. Eng. **29**, 183 (1987)
23. W. Ngantsoue-Hoc, Y. Zhang, R.J. O'Brien, M. Luo, B.H. Davis, Appl. Catal. **236**, 77 (2002)
24. X. Wang, Q. Zhang, S. Yang, Y. Wang, J. Phys. Chem. B **109**, 23500 (2005)
25. C. Yu, B. Tian, J. Fan, G.D. Stucky, D. Zhao, Chem. Commun. **24**, 2726 (2001)
26. T. Zhang, R. Wang, W. Geng, X. Li, Q. Qi, Y. He, S. Wang, Sens. Actuators B Chem. **128**, 482 (2008)
27. K.S.W. Sing, D.H. Everett, R.A.W. Haul, L. Moscou, R.A. Pierotti, J. Rouquerol, T. Siemieniewska, Pure Appl. Chem. **57**, 603 (1985)
28. J.M. Esparza, M.L. Ojeda, A. Campero, A. Domínguez, I. Kornhauser, F. Rojas, A.M. Vidales, R.H. López, G. Zgrablich, Colloids Surf. A Physicochem. Eng. Asp. **241**, 35 (2004)
29. Y. Wang, F. Zhang, Y. Wang, J. Ren, C. Li, X. Liu, Y. Guo, Y. Guo, G. Lu, Mater. Chem. Phys. **115**, 649 (2009)
30. B. Pawelec, P. Castaño, J.M. Arandes, J. Bilbao, S. Thomas, M.A. Peña, J.L. Garcia, Fierro. Appl. Catal. A **317**, 20 (2007)
31. A. Miyakoshi, A. Ueno, M. Ichikawa, Appl. Catal. A **219**, 249 (2001)
32. M.L. Ruiz, I.D. Lick, M.I. Ponzi, E. Rodriguez-Castellón, A. Jiménez-López, E.N. Ponzi, Appl. Catal. A **392**, 45 (2010)
33. V.K. Díez, C.R. Apesteguía, J.I. Di Cosimo, Catal. Today **63**, 53 (2000)
34. J.H. Zhu, Y. Chun, Y. Wang, Q.H. Xu, Mater. Lett. **33**, 207 (1997)